Separation and Purification Technology 342 (2024) 126860

Contents lists available at ScienceDirect

Separation and Purification Technology

journal homepage: www.elsevier.com/locate/seppur

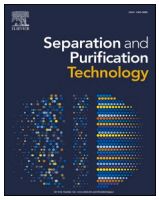

Understanding electrostatic interaction on strong cation-exchanger via co-ion valency effects

G.M. Essert [a,*], J.P. de Souza [b], S.P. Schwaminger [a,c,d], M.Z. Bazant [b,e], S. Berensmeier [a,f,*]

[a] Chair of Bioseparation Engineering, TUM School of Engineering and Design, Department of Energy and Process Engineering, Technical University of Munich, Garching 85748, Germany
[b] Department of Chemical Engineering, Massachusetts Institute of Technology, Cambridge, MA 02139, United States
[c] Division of Medicinal Chemistry, Otto Loewi Research Center, Medical University of Graz, Graz 8010, Austria
[d] BioTechMed-Graz, Graz 8010, Austria
[e] Department of Mathematics, Massachusetts Institute of Technology, Cambridge, MA 02139, United States
[f] Munich Institute of Integrated Materials, Energy and Process Engineering, Technical University of Munich, 85748 Garching, Germany

A B S T R A C T

Empirical adsorption models have been extensively used to design and optimize ion exchange chromatography (IEC) processes for proteins. The equations go 40 years back to the qualitative findings about the electrical double layer (EDL) in ion exchangers and form the basis of the stoichiometric displacement (SD) model widely used in preparative chromatography. While the SD model reduces the experimental effort to find salt-eluting conditions for the separation, knowledge transfer is restricted from one system to another. However, this limitation can be overcome by understanding the physicochemical interaction mechanism between the solid adsorbent and the electrolyte. Via a theoretical and experimental approach, we investigated the physicochemical adsorption mechanism in IEC and developed a methodology to determine it quantitatively by measuring the effective EDL thickness. We performed negative adsorption experiments in high-performance liquid chromatography to measure the excluded volume of co-ions, citrate, or oxalate on strong cation exchange resin. Together with the physical specifications of the column and the deployment of a modified nonlinear Poisson-Boltzmann equation, we identified the effects of the electrolyte composition on the size of the EDL. While it depends on the concentration, valency, and size of the counterion, we derived that the expansion of the EDL is indicated by different valencies of the carboxylate co-ions in trace amounts. Our findings provide a self-consistent theory of the transport phenomena in a solid/fluid system with all parameters specified with the physical properties of the chromatographic process. Further, optimizing the resin design or improving the adsorption and desorption conditions for biomolecules may be facilitated. Altogether, our work may improve material designing and process development and, thereby, help to overcome the concurrent technological and economic bottlenecks of the well-deployed purification step of IEC.

1. Introduction

Ion exchange chromatography (IEC) is essential for the production of biotherapeutics, as well as other separation technologies. Models of IEC can be traced to the middle of the past century, notably to the early work of Neal Amundson [1–3], the “father of modern chemical engineering” [4,5]. For the past 40 years, process development in preparative ion exchange chromatography of proteins has heavily relied on the findings of Kopaciewicz and co-workers about adsorption [6]. The authors [7] formulated the well-known stoichiometric displacement (SD) model, which has been very useful to experimentally characterize the adsorption of differently charged proteins on the stationary phase. In the empirical SD model, ion exchange is described by a stoichiometric relationship of a characteristic charge of the protein with the salt concentration in the eluent. Nevertheless, the authors deduced the empirical SD model from electrostatic interaction experiments that they qualitatively rationalized with the existence of the electrical double layer (EDL). These unconventional experiments differed from typical ion exclusion chromatography. They quantified the exclusion volume of ions in chromatography, which carry the same charge as the stationary phase, depending on the ionic strength of the buffer in the mobile phase. Thus, revisiting these principal investigations - the foundation of the successful SD model - and building current investigations upon them appears very promising for expanding our understanding of adsorption in IEC; since, accurate adsorption models are still the technological and economic bottleneck in process development of ion exchange chromatography [6,8,9].

The great benefit of understanding the adsorption mechanism can be emphasized through similar technical processes that already exist in the field of environmental engineering and water remediation. The flow-

* Corresponding authors at: Chair of Bioseparation Engineering, TUM School of Engineering and Design, Department of Energy and Process Engineering, Technical University of Munich, Garching 85748, Germany (G.M. Essert and S. Berensmeier).
E-mail addresses: g.essert@tum.de (G.M. Essert), s.berensmeier@tum.de (S. Berensmeier).

https://doi.org/10.1016/j.seppur.2024.126860
Received 25 January 2024; Accepted 19 February 2024
Available online 27 February 2024

through processes have been optimized towards or built on effective surface exchange by deployment of the EDL theory. Thereby, the different process concepts can be subdivided on the basis of pore sizes that influence the modeling of the double layer. Microporous adsorption of monovalent neutral salt with Langmuir-type surface charge regulation has been derived in dynamic water desalination processes, experimentally and through analytical mathematical expression [10–16]. Further developed systems include an elevated surface potential due to permanent surface charges [13] and redox-active charges [15]. Moreover, physics-based simulations of capacitive deionization rationalized process dynamics, with a binary mixture of monovalent ions [17], of monovalent and divalent ions [18,19], and solutions including an organic acid that underlies water association reactions [20]. In electrochemical processes including shock electrodialysis, the different charging behavior of the EDL with divalent or monovalent counterions in macroporous materials has been exploited [21–25]. Ultimately, a more in depth-understanding of the transport mechanism resolved pore-scale effects that alter macroscopic separations [26,27]. Elucidating subtle effects of multivalent ions and water associations reactions facilitated metal ion separations leveraging pH swings in shock electrodialysis, where pH-dependent complexation reactions modify and even change the sign of multivalent cations in solution including the conversion of multivalent cations into oxyanions [28]. Such quantitative insights to the electrosorption process could also be relevant for ion-exchange chromatography where the separation is dominated by charge-surface interactions.

Kopaciewicz *et al.* [7] investigated a macroporous system of small analytes and ion exchange material of great pore size via electrostatic interactions experiments but did not quantify their observation in consideration of the electrolyte composition. In this work, we give detailed insights on the electrostatic interaction of the electrolyte with multiple ion species in a strong cation-exchanger. As in Kopaciewicz's work, we perform interaction studies via chromatography with a macroporous resin and, examine a great range of ionic strength of a phosphate buffer to ensure consistency with the mechanism (Section 4.1). Our aim is to extend the picture of electrostatic interaction in ion chromatography by a more direct quantification of the experimental results in terms of the EDL structure compared to the work by Kopaciewicz *et al.* In doing so, we deploy the mathematical formulation of the continuum-based EDL theory. Consequently, we relate the size of the EDL not only to a specific type of the stationary phase and a specific type of the buffer - as the load of the resin in an empirical adsorption isotherm is related to the specific resin and a specific buffer condition, which restricts knowledge transfer from one system to another - but to general physical characteristics of the system. These characteristics are the surface charge density of the stationary phase and the ion identities of the electrolyte. Concretely, we consider the concentration, valency and size of the counterions to the surface charge and the concentration and valency of the co-ions. In other words, we carefully take into account the water association reactions of buffer ions and analytes. As we investigate three different buffer conditions, the molar ratio of protonated to dissociated species is different. In the end, our experimental and theoretical results lead to a methodology to determine the effective size of the EDL. The methodology is useful to understand the electrostatic interaction of different solid materials with different electrolytes in chromatography that in turn can be useful for designing solid materials and controlling the adsorption of charged biomolecules.

To investigate the physicochemical adsorption mechanism, we deploy a modified nonlinear Poisson-Boltzmann equation to explain the adsorption of positively monovalent counterions and repulsion of charged co-ions of different negative valency. Here, the valency of the co-ions varies with the ionic strength and pH of the buffer. The continuum-based adsorption model is used to quantitatively describe the structure of the double layer and the excluded volume of oxalate and citrate charge species from the highly negatively charged stationary phase (Section 4.2). Eventually, the degree of repulsion depends on the electrolyte composition and is quantified via the double layer theory (Sections 4.2.2–4.2.4). All the model parameters are determined by direct measurements or from literature values. (Section 4.2.1). Since all the parameters are specified, no parameter estimation is needed to describe the chromatographic process.

Eventually, the greater the repulsion the greater the size of the double layer. In Section 4.2.6, we discuss how the greater expansion of the double layer increases the interaction range for potential adsorption of charged biomolecules. Further, the lower the expansion of the double layer the more favorable is the desorption of the oppositely charged protein. This case is discussed in Section 4.2.5 and shows the case that Kopaciewicz *et al.* observed for proteins under eluting conditions and described with their empirical SD model.

By understanding the interfacial electrolyte structure, we want to advance this current empirical picture. We believe that a better understanding of the adsorption mechanism in ion chromatography will be useful to base the separation process on optimal surface exchange as it has been beneficial in similar technical applications [24]. Via the model with specified parameters, the size of the EDL can be determined – directly in the dynamic chromatographic process and under actual buffer conditions – by considering the surface charge density of the resin, the concentration, size and valency of the counterions and, the concentration and valency of the co-ions.

2. Theory

In this work, experimental retention times of co-ions in chromatography are explained by the EDL theory. As co-ions have the same charge as the stationary phase, they are repelled from its surface. The description of the transport phenomena is based on the ideal model of chromatography in combination with quasi-equilibrium electrosorption. Concretely, we derive differential partition coefficients with units of length from experimental retention times and compare them with the effective thickness of the double layer. The expansion of the double layer depends on the composition of the electrolyte and is defined by a modified Poisson-Boltzmann theory. The theory describes the accumulation of counterions and the decrease of co-ions near to the surface in comparison to the bulk concentration further away. Hence, counterions are adsorbed to the surface while co-ions are repelled and negatively adsorbed [29,30].

2.1. Electrostatic adsorption in chromatography

As we are interested in the retention times, the ideal chromatography model is adequate to describe the mass balance in the mobile phase. Neglecting axial dispersion and mass transfer and, assuming instantaneous adsorption equilibrium, the local concentration of solute c_i (mol m^{-3}) in the chromatographic column is described by [31],

$$\phi \frac{\partial c_i}{\partial t} + S \frac{\partial q_i}{\partial t} + \phi u \frac{\partial c_i}{\partial z} = 0 \tag{1}$$

when u (m s^{-1}) is the local average mobile phase velocity and, ϕ (−) is the porosity, the ratio of the void volume to column volume (CV). Compared to the literature, we redefine q_i, the equilibrium concentration of component i on the stationary phase. Instead of relating the molar mass of the adsorbed species to the volume of the stationary phase in the column (column volume), we relate it to the surface area of the stationary phase in the column and obtain q_i (mol m^{-2}). Consequently, the phase ratio is reformulated as S (m^{-1}), the ratio of the surface area of the stationary phase to the column volume. As we divide by porosity ϕ, we obtain S/ϕ, surface area per volume of mobile phase which has also been defined in a well-known work about experimental characterization of ion-exchangers [32].

Once we assume quasi-equilibrium of the adsorption and independence of the adsorption from hydrodynamics, the concentration in the

stationary phase depends on the local concentration in the mobile phase, $\partial q_i/\partial c_i = (\partial q_i/\partial t)/(\partial c_i/dt)$, we derive

$$\frac{\partial c_i}{\partial t} + \frac{u}{1+\frac{S}{\phi}\frac{dq_i}{dc_i}}\frac{\partial c_i}{\partial z} = 0 \tag{2}$$

and point out that the solute concentration travels axially (direction z) through the column while depending on the adsorption equilibrium. Therefore, solutes with different adsorption equilibria evolve through the column with different speed that result in different retention times.

Stated the other way around, the adsorption equilibrium can be determined by the retention time t_i (s). When we reference the retention times to a non-adsorbing species, which is only influenced by hydrodynamic interaction without adsorption, we are able to quantify the adsorption equilibria of different solutes. As the inert solute travels through the column of length L with

$$t_{ref} = \frac{L}{u} \tag{3}$$

via Eq. (2), we determine the differential partitioning coefficient of the adsorption equilibrium

$$\frac{t_i - t_{ref}}{t_{ref}} = \frac{S}{\phi}\frac{dq_i}{dc_i} \tag{4}$$

When the concentration perturbation of the solutes is small enough such that adsorption is linear, no shocks or discontinuities emerge. For the differential partitioning coefficient, we finally obtain

$$\ell_{exp} = \left(\frac{dq_i}{dc_i}\right)_{exp} = \frac{\phi}{S}\left(\frac{t_i - t_{ref}}{t_{ref}}\right) \tag{5}$$

and define length ℓ_{exp} (m) that is experimentally derived by the retention time shift. Effectively, porosity of the column ϕ and the dead time of the plant t_{dead} cancel out (see Eq. S1 in Supporting Information). Latter is the measured time from the injector to the detector of the plant when the chromatographic column is removed. In Eq. (5), positive length values relate to positive differential partitioning coefficients and greater retention times of the solute than the inert species. The solute adsorbs to the stationary phase. Negative length values correspond to negative differential partitioning coefficients, which means faster elution times of the interacting solute compared to the inert species. Consequently, the solute experiences negative adsorption, which corresponds to less fluid volume that is accessible to the solute in comparison to the inert species. The negative adsorption configuration is not the typical configuration of IEC processes, but the negative adsorption provides valuable information about the underlying electrosorption phenomenon. Such observations supported the formulation of the SD model.

2.2. Electrical double layer theory via nonlinear modified Poisson-Boltzmann equation

The electrical double layer theory describes the electrostatic screening of a charged surface by accumulated counterions and depleted co-ions in the vicinity of the surface that both differ from the bulk electrolyte concentration far away from the surface. The counterions carry the opposite charge to the surface, while the co-ions are of like-charge. Unspecific attraction of the counterions and unspecific repulsion of co-ions occurs diffusely near the interface due to the electric field distribution in the double layer that counteracts the entropy of mixing. On the other hand, specific interactions of the solvent and ions with the surface are accounted for by the compact Stern layer that lies between the surface and the diffuse layer [33].

In this work, we neglect specific interactions as the physical parameters that we determine experimentally account for the diffuse layer. Therefore, the interactions of the solutes provoked by the electrostatic field are reversible and unspecific. Beyond the dilute Poisson-Boltzmann theory, we consider a modified Poisson-Boltzmann equation (Eq. (6), equivalent to the original mean-field theory of Bikerman [34], which accounts for ion crowding at highly charged surfaces within a lattice-gas approximation, as first proposed by Grimley and Mott for solid electrolytes [35]. Regardless of the details of the model, at highly charged surfaces, the structure of the double layer is strongly affected by counterion crowding, which is dependent on the ionic characteristics including the ion valency and ion size [34,36].

In this work, all ion sizes are assumed equal here since the most important packing effect comes from the counterions, although extensions to asymmetric systems are possible [37–39]. The modified Poisson-Boltzmann equation is:

$$(\varepsilon\psi')' = \frac{-eN_A\sum z_i e c_{0,i}\exp\left(-\frac{z_i e\psi}{kT}\right)}{1+\sum \upsilon c_{0,i}\left[\exp\left(-\frac{z_i e\psi}{kT}\right)-1\right]} \tag{6}$$

The model describes the relationship of ions with valency z_i (−) and equilibrium concentration in the bulk $c_{0,i}$ (mol m^{-3}) far away from the surface with the potential ψ (V). Other parameters are natural constants and macroscopic system parameters. There is the product ε of the dielectric constant of water and the vacuum permittivity ($80 \cdot 8.85 \cdot 10^{-12}$ C V^{-1} m^{-1}), which is assumed to be constant, the elementary charge e ($1.6 \cdot 10^{-19}$ C), the Boltzmann constant k ($1.38 \cdot 10^{-23}$ J K^{-1}) and the absolute temperature T (300 K), respectively. Further, a steric factor υ (m^3 mol^{-1}) accounts for ion crowding of solvated counterions of radius a (m) and follows $\upsilon = \frac{4}{3}\pi a^3 N_A/p$ with Avogadro number N_A ($6.022 \cdot 10^{23}$ mol^{-1}) and, packing density $p = 0.52$ for random close packing. This parameter could be adjusted to capture slightly higher packing fractions of random close packing ($p = 0.64$) or close packing on a lattice ($p = 0.74$) [40]. For $\upsilon = 0$, the Bikerman model reduces to the Poisson-Boltzmann equation. Moreover, we assume electroneutrality of the double layer as the condensed and diffuse layer compensate the charge density of the surface.

Once we make the mean-field approximation and non-dimensionalize the modified Poisson-Boltzmann equation (Eq. (6)) by scaling to the Debye length $\lambda_D = \sqrt{kT\varepsilon/\left(e^2 N_A\sum_i z_i^2 c_{0,i}\right)}$, we obtain

$$\tilde{\psi}'' = \frac{\sum \frac{z_i c_{0,i}}{\sum z_i^2 c_{0,i}}\exp(-z_i\tilde{\psi})}{1+\sum \upsilon c_{0,i}[\exp(-z_i\tilde{\psi})-1]} \tag{7}$$

To solve the nonlinear second-order differential equation numerically, two boundary conditions are necessary. These are based on the exchanger charge and the bulk conditions.

2.3. Boundary conditions

Once we determine the ionic capacity of the material through the specifications of the chromatographic column, we are able to define the surface charge density as one boundary condition. The second boundary condition is of Dirichlet type at far distances from the surface, where the potential is set to zero.

The ionic capacity of the column is determined by the equilibration of the ion-exchanger with protons and subsequent exchange by a neutral salt. During the procedure, the protons are captured and are quantified via pH-meter and via titration afterwards. The concentration c_t (mol m^{-3}) and the volume V_t (m^3) of the base titrant result in the amount of hydronium ions as monovalent counterions. According to Eq. (8), we can calculate ionic capacity Λ (meq g^{-1}) of the strong cation exchange material in the column with volume V_{col} (m^3) and bed density ρ_{bed} (g m^{-3})

$$\Lambda = 10^3\frac{meq}{mol}\cdot\frac{c_t V_t}{\rho_{bed} V_{col}} \tag{8}$$

Via Eq. (9) and through the specific surface area A_s (m^2 g^{-1}), we

calculate the amount of ions adsorbed to the material as the area-related ionic capacity and define it as surface charge density σ^d_{exp} (C m^{-2}).

$$(\sigma^d)_{exp} = \frac{\Lambda e N_A}{10^3 \frac{meq}{mol} \cdot A_s} \tag{9}$$

Since the material is a strong cation exchange resin, the surface charge does not change with the concentration of the protons over the pH range of the experiments [41]. Consequently, we define the boundary condition on the surface to be of Neumann type using Gauss' law [33] and obtain

$$\left(\frac{d\tilde{\psi}}{d\tilde{x}}\right)\Big|_{\tilde{x}=0} = \frac{\lambda_D e}{kT}\left(\frac{d\psi}{dx}\right)\Big|_{x=0} \equiv -\frac{\lambda_D e}{kT}\frac{1}{\varepsilon_0 \varepsilon}(\sigma^d)_{exp} \tag{10}$$

2.4. Negative adsorption of co-ions

From the solution of the modified Poisson-Boltzmann equation, the surface excess concentration q_i of species i in the double layer can be calculated. For a negatively charged surface, the accumulation of counterions and depletion of co-ions follows the surface potential:

$$q_i = \int_0^\infty (c_i - c_{0,i})dx = \int_0^\infty \left(\frac{c_{0,i}\exp(-z_i\tilde{\psi})}{1+\sum \nu c_{0,i}[\exp(-z_i\tilde{\psi})-1]} - c_{0,i}\right)dx \tag{11}$$

In case of cations on the negatively charged surface, the term $-z_i\tilde{\psi} > 0$, and therefore holds $q_i > 0$. On the other hand, co-ions follow $-z_i\tilde{\psi} < 0$ and the surface excess concentration is negative. From there, we are able to calculate numerically the differential partition coefficient of the repelled co-ion,

$$\ell_{theory} = \left(\frac{dq_i}{dc_i}\right)_{theory} \tag{12}$$

which has the units of length and has a negative sign. Through this expression, we are able to bring together the adsorption equilibrium proposed by the double layer structure with the adsorption equilibrium derived from the retention times in chromatography (Section 2.1). While the adsorption of the solute can be linear, it depends nonlinearly on the double layer structure. Thereby, we assume that the bulk concentration is in quasi-equilibrium with the double layer at the surface. Further, we neglect overlapping of double layers within pores and the complexities of electrokinetics. Here, electrostatic potential gradients at the pore scale are decreased by the presence of a supporting electrolyte buffer which allows us to consider the depletion of individual ionic species independently.

The supporting electrolyte suppresses electromigration of the ionic species. As the ion concentration of the supporting electrolyte is greater than those of the co-ions of interest, the macroscopic pore-scale potential is minimized [42].

From Eq. (11) and Eq. (12), the model predicts that different co-ion valencies lead to different retention time shifts. Therefore, a pulse as it evolves through the column, will eventually split into two populations according to the valencies, although in a dynamic manner, these pulses will be subject to the local chemical equilibrium of the given ionic species.

In Fig. 1, the principle of negative adsorption on the stationary phase in the chromatographic column is visualized. Higher charged species of citrate are more repelled from the surface than lower charged species according to the double layer structure, which is determined by crowding and accumulation of counterions on the highly charged surface.

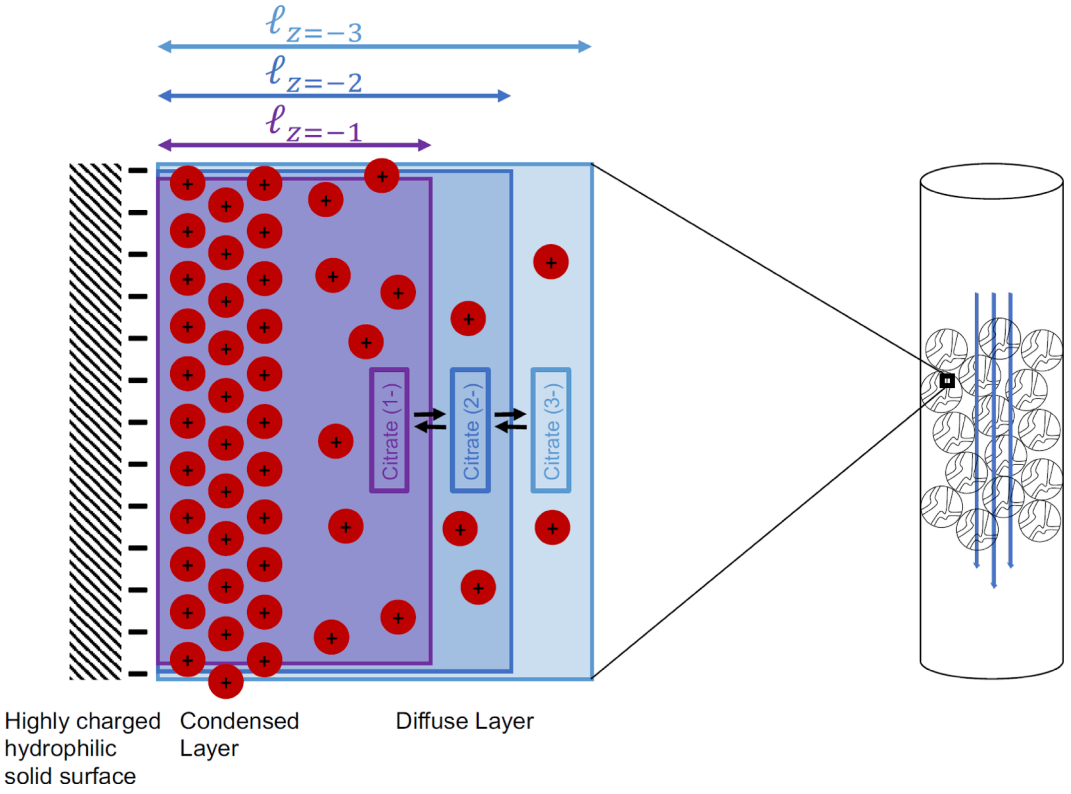

Fig. 1. Repulsion of different citrate charge species from the surface according to the double layer theory as negative adsorption equilibrium in chromatography. Positively charged counterions screen the highly negatively charged hydrophilic surface in a condensed and a diffuse layer. Negatively charged citrate co-ions are repelled according to their valency. The higher the co-ion valency z, the greater is the excluded distance ℓ from the surface corresponding to a greater excluded volume in the three-dimensional chromatographic column.

3. Materials and methods

3.1. Negative adsorption experiments

Negative adsorption experiments were performed in a strong cation exchange column (PL-SCX 1000 Å, 150 mm × 4.6 mm, 0.39 g mL^{-1}, 10 μm) (Agilent, Cheadle, UK) under varying ionic strengths from 0.002 to 0.278 M and pH 6, 7 and 8 of phosphate with monovalent potassium, as counter-ion, as buffer and supporting electrolyte.

Potassium phosphate buffer was manufactured by weighting di-potassium hydrogen phosphate (VWR, Leuven, Belgium) and potassium phosphate monobasic (VWR, Leuven, Belgium) to reach different ionic strengths and pH values. No addition of other ions was performed to adjust the pH. Samples were prepared with the according buffer and different concentrations of potassium citrate (Carl Roth, Karlsruhe, Germany) or glucose (AppliChem, Darmstadt, Germany). Samples of potassium oxalate were made by addition of potassium hydroxide (Sigma Aldrich, Steinheim, Germany) and oxalic acid (Sigma Aldrich, Steinheim, Germany) to the buffer. Buffers used for chromatography were filtered (0.2 μm ∅) and degassed, samples were filtered.

Chromatography was performed in an Agilent 1100 Series HPLC system at 0.5 mL min^{-1} and 27–30 °C with different buffer conditions. Inject volume of the samples is 5 μL and the elution of the species is measured via refractive index detector (G1362A, Agilent, Santa Clara, CA, USA).

In Table 1, the acid dissociation constants of the buffer and the analytes are listed to better follow the discussion of the results.

3.2. Ionic capacity

The ionic capacity of the strong cation exchange column was obtained in the Agilent 1260 Infinity II. Therefore, the column was transferred in its H-form and eventually the amount of bound ions was quantified via titration of a base. We equilibrated the column with 0.5 M HCl, prepared from stock solution (37 %, VWR, Leuven, Belgium), for 5 CV followed by flushing of DI water for another 5 CV to elute unbound protons. The equilibration times are in accordance with the supplier's user manual. Subsequently, we rinsed with 1 M KCl, manufactured from weighting the solid (Grüssing, Filsum, Germany), for 12 CV to assure the complete elution of protons. During the procedure, we collected the effluent from the column in an Eppendorf flask. Before application, the solutions were sterile filtered.

The effluent was titrated with 0.1 M KOH, prepared from weighing the solid (Sigma-Aldrich, Steinheim, Germany), until the collected hydronium ions were neutralized at pH 7. We used a pH-meter Lab 845 (SI Analytics, Rye Brook, NY, USA) to track occurrence of the transition point and to confirm the calculated amount of hydronium ions by measuring the effluent before titration.

3.3. Specific surface area

The specific surface area was determined with a Gemini VII 2390 Surface Area Analyzer (Micromeritics Instrument Corporation, Norcross, GA, USA). Prior to analysis, the samples were dried in vacuum at 100 °C and weighed. The measurement included a determination of the sample volume with the inert gas helium and the gas adsorption isotherm of nitrogen at 77 K. The range of the relative pressure was 0.05 to 0.25. From the gas adsorption isotherms, the specific surface area was determined by the BET-method.

Table 1
Acid dissociation constants of species in the investigated electrolyte.

Chemicals	Acid Dissociation Constants		
	pKa_1	pKa_2	pKa_3
Phosphate [43]	2.15	7.09	12.32
Citrate [44]	3.13	4.76	6.40
Oxalate [45]	1.46	4.40	–

3.4. Computation

Calculations were performed in Matlab R2021b. The solver bvp4c was used to numerically solve the modified Poisson-Boltzmann equation.

4. Results and discussion

4.1. Dynamic negative adsorption on ion exchange resin in potassium phosphate buffer

The high throughput approach in the HPLC system enables an effective way to investigate the electrostatic interaction of the resin under variation of the mobile phase conditions in terms of ionic strength and pH. The apparent negative adsorption of injected carboxylic acids as co-ions is highly significant and reproducible, as it will be set out in detail in the results section. Consequently, it indicates a high sensitivity of this measurement method.

As in the pioneering work of Kopaciewicz *et al.* [7], we investigate the negative adsorption of citrate and oxalate with potassium phosphate buffer at pH 6, however, extend it to buffer values of pH 7 and 8 and lay out the chromatograms in detail. Actually, at pH 7 and 8, phosphate works as a buffer as it is close to its pKa_2 value compared to weak buffer conditions at pH 6. The counterion is monovalent potassium, as it is in the mobile phase and in the injected sample with oxalate and citrate. These negatively adsorbed species indicate the size of the electric double layer when related to uncharged glucose, which does not electrostatically interact with the surface and permeates the complete fluid volume. The investigated resin has a large pore size to show the electrostatic effects also in relevance to chromatography of biomolecules of greater size while size exclusion of the small analytes is prevented. As well, the sufficiently wide pore sizes avoid the formation of the Donnan potential of the pore volume, so that the negative adsorption appears on the surface within the pores as deduced from a more detailed discussion in Section 4.2.6.

4.1.1. Four aspects of co-ion repulsion in chromatography

Fig. 2 includes chromatograms of six (four) injected samples, triplicates (duplicates) of oxalate and glucose, under isocratic conditions with potassium phosphate at pH 6. We find measurements with ionic strength of the buffer of 0.01 M and 0.1 M and locate the signal of the detector (nRIU) for process times of 4.5 min. The chromatograms represent an expanded dataset consisting of more technical replicates and varying values of ionic strength. The overlap of the chromatograms shows high reproducibility, and point to the high significance of the retention times of the analytes. The prior elution of oxalate compared to glucose indicates the negative adsorption of the carboxylic acid, which is a measure of the expansion of the electric double layer. In other words, due to ion exclusion, less volume is accessible to the like-charge co-ion to the surface than to the uncharged glucose. As we compare the upper and lower chromatograms, we point out the extent of the adsorption depends on the composition of the mobile phase. When referencing to the retention time of glucose, we derive different shifts of the major signal with -0.43 ± 0.01 min and -0.27 ± 0.02 min at the ionic strength 0.01 M and 0.1 M, respectively.

In the chromatograms, some irregular perturbation of the oxalate and the glucose signal, including negative RI values, appears around the retention time of oxalate's major peak. These derive from subtracting buffer blanks from the analyte signal to diminish the injection event. On the other hand, the consistent small peak ahead of the major oxalate signal also derives from electrostatic repulsion, as we further elaborate in comparison with the citrate results. Remarkably, at great repulsion, elution of the co-ion even takes place, before the injection event is

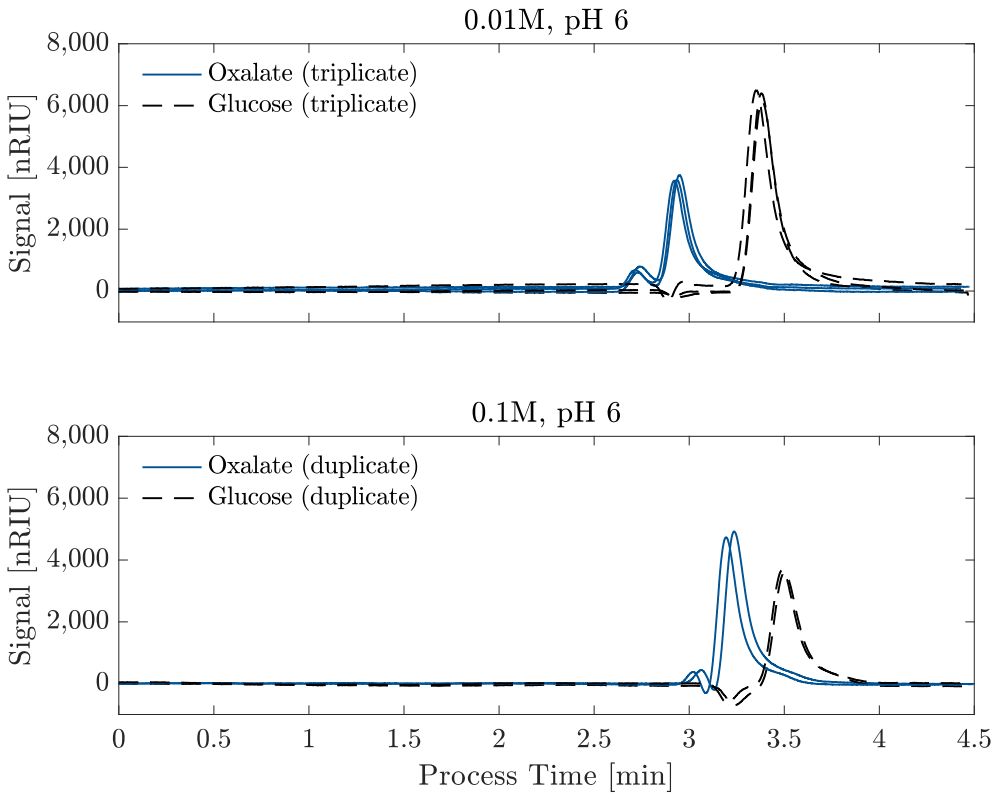

Fig. 2. Two compiled chromatograms with negatively adsorbed oxalate and permeating glucose. Increasing ion strength from 0.01 M phosphate buffer to 0.1 M leads to a significant change of the elution time shift from -0.27 ± 0.02 to -0.43 ± 0.01 min when referenced to glucose, respectively. Duplicates and triplicates of samples with 2.7 mM potassium oxalate or 2.5 mM glucose are demonstrated representatively. Average values and standard deviations stem from additional technical replicates, which involve additional chromatographic runs of injected samples at various oxalate concentrations. Inject volume: 5 µL. Flow rate: 0.5 mL min^{-1}. Signals after subtraction of buffer blank.

visible in the chromatogram.

Fig. 3 contains chromatograms of four (six) injected samples, representative duplicates (triplicates) of citrate and glucose under isocratic conditions with potassium phosphate with ionic strength of 0.1 M at pH 6 and 8, respectively. In both cases, the injection of citrate leads to two great signals that together hold information about the thickness of the EDL. The two peaks form due to the equilibrium of different charged species of the co-ion. In the next paragraphs, we will carefully divide apart four qualitative aspects in what way the carboxylic acids indicate double layer expansion. In Section 4.2, the consideration of more experimental results together with the theory will explain them quantitatively.

As we compare the citrate peaks at pH 8 and at pH 6 (Fig. 3), we see that latter ones have lower elution times at first sight. After referencing to glucose, respectively, the shift of the second peak at pH 8 results in -0.33 ± 0.03 min and is slightly greater than at pH 6 (-0.28 ± 0.01 min), while the shifts of the first peaks are the same with -0.46 ± 0.02 min at pH 8 and -0.47 ± 0.03 min at pH 6. As these shift quantities show barely a difference, they are still not the same, and indeed, four qualitative differences influence the signals.

First, at exactly 0.111 M ionic strength, the buffer at pH 8 consists of 76 mM potassium ions, while at exactly 0.115 M at pH 6, it consists of 108 mM potassium ions. As the counterion at these mediate concentrations sensitively determines the thickness of the electrical double layer, the double layer at pH 8 is greater than at pH 6. However, the retention time shifts of the first citrate peaks indicate otherwise. The shifts are almost the same, what actually would indicate almost equal double layer thicknesses.

The second effect influences the shift in the opposite way, so that it apparently almost neutralizes the first effect. Due to the different pH values, different species of citrate form. At pH 8, almost all the co-ions are trivalent, while at pH 6, more divalent than trivalent citrate ions are theoretically prevalent. As co-ions of higher valency are more expelled, the effective double layer expansion for the higher valency ions apparently is greater. Consequently, to measure the thickness of the EDL, the co-ion valency has to be considered. Later, the theory incorporates these qualities by incorporating the formation of the electrical double layer and the implicit negative adsorption of the co-ion species of different valency.

Moreover, clearly visible is the occurrence of two peaks that indicate the thickness of the EDL. The peak splitting, the third effect, is a result of the prevalence of the two charge species of citrate at the investigated pH values. At pH 8, the trivalent citrate species is repelled from a greater volume than the divalent citrate species. Theoretically, the trivalent species and the divalent species diverge axially in the column if they did not form new equilibria with water according to the impact of the buffer. As the trivalent species go ahead, a new equilibrium of trivalent and divalent species establishes. The newly formed divalent species will be less repelled and slow down relatively to the trivalent ones. Then, they meet the trivalent ions that have been formed by the new equilibrium of the dragging divalent ions of the first population. Ultimately, the two peaks in the chromatogram can be understood as a manifestation of the equilibrium of trivalent and divalent citrate species, while both signals incorporate the same equilibrium. The underlying kinetics are complex and base on the kinetics of the water association reaction and the kinetics of electrostatic repulsion. In Section 4.2, we will describe the peak splitting by two limits of the theory: fast equilibrium and no equilibrium of the charged species.

The fourth qualitative aspect is the identification of the valencies. As the pH is close to the pKa value of the buffer, the charged co-ion species are prevalent according to the equilibrium constant of the buffer. At pH 8, mostly trivalent and few divalent citrate ions are prevalent. On the

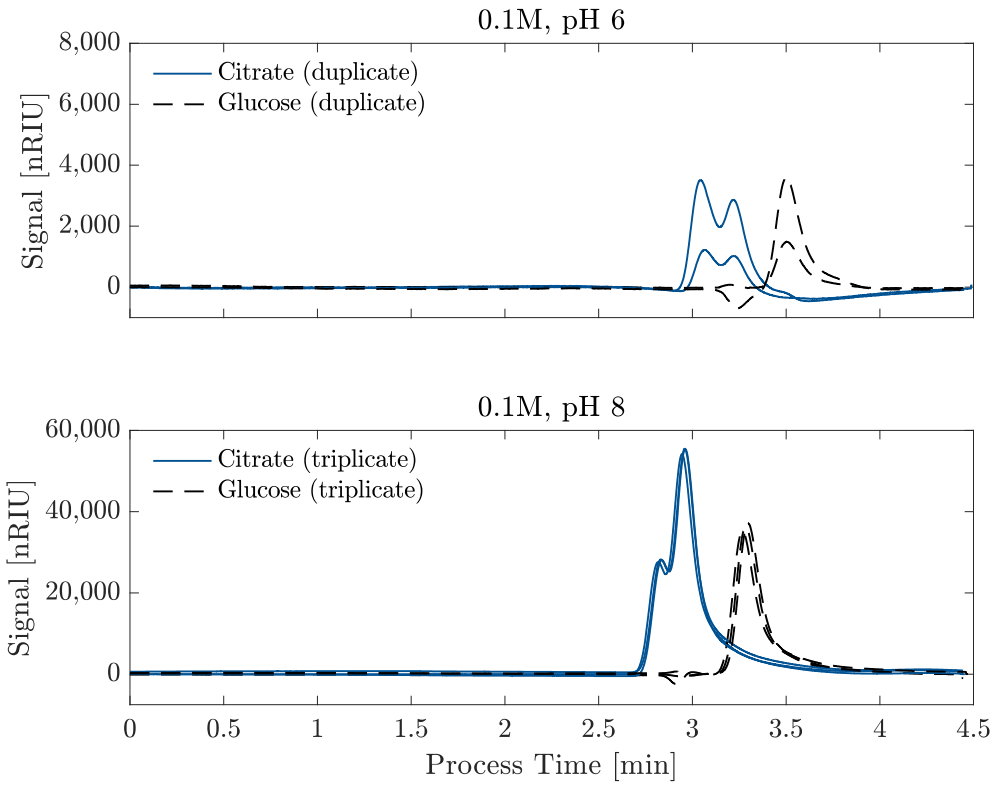

Fig. 3. Two compiled chromatograms with negatively adsorbed citrate and permeating glucose. Increasing pH value of phosphate buffer with ionic strength of 0.1 M from pH 6 to pH 8 leads to no change of the first of the double peaks with -0.47 ± 0.03 min and -0.46 ± 0.02 min, respectively. The elution time shift slightly changes from -0.28 ± 0.01 min at pH 6 to -0.33 ± 0.03 min at pH 8 when referenced to glucose, respectively. Duplicates of 1.0, 2.5 mM of potassium citrate or glucose and triplicates of samples with 30 mM potassium citrate or glucose are demonstrated representatively. Average values and standard deviations stem from additional technical replicates, which involve additional chromatographic runs of injected samples at various citrate concentrations. Inject volume: 5 µL. Flow rate: 0.5 mL min^{-1}. Signals after subtraction of buffer blank.

other hand, at pH 6, it is actually an equilibrium of divalent and monovalent citrate ions as we will thoroughly elaborate by comparing the results of citrate and oxalate in Section 4.1.2.

4.1.2. Determination of the extent of repulsion by co-ion valency

In comparison of citrate and oxalate at 0.1 M and pH 6 (Fig. 2 and Fig. 3), we point out that the shift of the second peaks is the same. At a closer look, also the shifts of the first citrate peak and the small first peak of oxalate are equal. This observation was also made at any other investigated ionic strength at pH 6. Here, it is to solve why monovalent oxalate and citrate species occur although the low pKa_2 values of 4.40 and 4.76, respectively, dictate otherwise. The reason is that phosphate at pH 6 is a weak buffer, and therefore the carboxylic acids establish monovalent charges to some extent as the differences to the pKa_2 values are not too great.

Ultimately, the match of the peaks are quite significant indications that on one hand, the two peaks imply the equilibrium of divalent and monovalent co-ions and on the other hand that the negative adsorption is not specific for one molecule but related to valency. One could hypothesize that the ratio of the peak area should follow the ratio of charged species in the equilibrium. However, the interplay of the four effects is very complex and such a distinction could not be made via the comparison of the peak areas. Lastly, for the comparison of the citrate results at pH 6 and pH 8, we conclude that two peaks of two different equilibria indicate the thickness of the electric double layer. At pH 8, the double layer expansion is indicated by two equilibria of trivalent and divalent citrate and at pH 6, by two equilibria of divalent and monovalent species.

The consideration of more experimental results will strengthen the statements. Together with the theory that quantitatively describes the peak splitting due to the establishment of different charged species in dependence on pH and ionic strength, we will give a coherent picture of the mechanism in Section 4.2.

4.1.3. Sensitivity analysis of species concentrations

Varying the analyte concentration, as exemplary demonstrated with 2.5 mM and 1 mM does not influence the retention times (Fig. 3). Higher concentrations may lead to lower resolutions, as we compare the peak splitting at pH 6 and pH 8. For low ionic strengths at pH 6, the injected concentration is more crucial. Clearly, high concentrations of potassium ions in the sample would locally affect the composition of the double layer. Further, as the concentration of the detected co-ions increases relatively to the concentration of the supporting electrolyte, which is the phosphate buffer, the contribution of electromigration to the transport phenomena may increase (see Section 2.4). Moreover, high concentrations of the injected carboxylic acid would compete with the weak phosphate buffer and influence the charge prevalence of the co-ions. Consistent results were obtained when the injected concentration of the carboxylic acid was maximally in parity at weak buffer conditions with pH 6 with ionic strengths of 0.01 M and lower (Supporting Information). Within this upper limit and the minimal resolution for identifying a peak from the baseline (order of 10^{-4} M), the repulsion was not sensitive to the variation of the carboxylic acid concentration in the sample.

As the injected pulse spreads out in the column due to axial dispersion, the effective equilibrium concentration is lower than the concentration in the sample and at least one order of magnitude lower than the concentration of the buffer. Therefore, in the concentration range of consistent results the contribution of the analyte to the ionic strength is neglectable as well as linear negative adsorption can be expected.

4.2. Quantification of electrical double layer thickness

After verification of the integrity of the physical parameters in Section 4.2.1, the adsorption mechanism in the chromatographic column is thoroughly described based on the quantification via the modified Poisson-Boltzmann theory. Hereby, the negative adsorption of oxalate (Section 4.2.2) and citrate (Sections 4.2.3 and 4.2.4) is outlined in dependence of the pH value and a great range of the ionic strength of the buffer. Subsequently, these fundamental findings are not only mapped to the elucidation of the functionality of the stoichiometric displacement model (Section 4.2.5) but also applied to resin design and, adsorption and desorption conditions of bioseparation systems (Section 4.2.6).

4.2.1. Verification of parameters: phase ratio, surface charge density and electrolyte species

We determined a phase ratio related to the mobile phase, S/ϕ, with 25 m^2 mL^{-1}, or 2.5 · 10^7 m^{-1} for the applied macroporous resin. The value lies in the order of magnitude of various reported cation exchange materials in the literature extracted from Table 1 and Table 3 in the work by DePhillips and Lenhoff [32]. Our value of 25 m^2 mL^{-1} agrees with that of all the tentacle-free and dextrane-free resins, which also have a reported pore size of 1000 Å by the manufacturers ([32], Table 1). All three cation exchange resins, based on a methacrylate matrix, fit perfectly with values of 23.1, 27.1 and 28.8 m^2 mL^{-1} while the value of non-functionalized silica with 13.8 m^2 mL^{-1} lies still in the same order of magnitude; these values apply to small molecules with molecular weights around 180 g mol^{-1} ([32], Table 3). In conclusion, the phase ratio that we determined for the applied cation exchange resin seems very reasonable; even so, in our case, the resin is based on a matrix of a polystyrene copolymer with a hydrophilic coating. Simultaneously, it supports our assumption, which was also made in the work by Kopaciewicz *et al.*, about high accessibility of the surface for carboxylate anions.

Finally, we obtain −58.4 μC cm^{-2} for the surface charge density; here, we determined experimentally the specific surface area and ionic capacity of the cation exchange material and considered the provided bed density by the manufacturer with 40 m^2 g^{-1}, 0.24 meq g^{-1} and 0.39 g mL^{-1} respectively. The calculated ion exchange capacity of 0.24 meq g^{-1} agrees with those that other manufacturers provide [41]. The integrity of the determined value of the surface charge density, the ion exchange capacity in terms of area, is verified by additional literature; since functionalized groups are synthesized onto the surface, we expected and consequently demonstrate elevated surface charge densities of the investigated material compared to bare, non-functionalized materials exhibiting only few μC cm^{-2} [33]. The order of magnitude that we determined agrees with high surface charge densities of strong cation-exchangers that have been reported elsewhere [46].

For the experimental determination of the surface charge density in chromatography, the amount of bound protons is defined as the amount that is adsorbed to the surface when in equilibrium with DI water; therefore, the column is transitioned into its H-form, and subsequently, flushed with DI water. The step of rinsing guarantees that the bulk is replaced by water and unbound protons in the interstitial and the pore bulk volume from the prior transition step are removed. Otherwise, the ionic capacity would erroneously lead to higher values. As fresh water flushes the column and diffuses into pores during equilibration, protons remain bound to the highly negative surface while the bulk concentration stays negligible. Finally, we quantify the amount of these ions by exchanging them with a neutral salt and then conducting an acid-base titration. This allows us to determine both the ionic capacity and, in combination with the specific surface area, the surface charge density of the double layer.

In the theoretical picture, we are aware that highly charged surfaces provoke specific interactions; here, a compact layer of solvent molecules and specific ion interactions emerge in the form of a Stern-Layer. However, we only address the effects of high surface charge that are reversible in the form of ion crowding as we consider a condensed layer between the surface and the diffuse layer. Ion exchange chromatography is a reversible process and therefore, non-specific electrostatic adsorption in the condensed and diffuse layer is of primary interest. As the incorporation of ion crowding is crucial to describe adsorption at highly charged surfaces, the size of hydrated potassium is considered, with a = 3.3 Å [47]. The co-ions are probably of larger size, but we are not accounting for ion size asymmetry in the model. Consequently, the microscopic size of the counterion is linked to the macroscopic process of chromatography.

Furthermore, we derive the equilibrium concentrations of potassium and the anions via the Henderson-Hasselbalch equation according to acid dissociation constants in Table 1 and, consider the ratios of the charged species in the calculations with the modified Poisson-Boltzmann equation (Eq. (6)).

4.2.2. Elucidation of transport phenomena: repulsion of oxalate

The thickness of the EDL is determined by the counterion and, as we lined out, can be measured by the degree of repulsion of co-ions. Our mechanistic model quantifies the interactions of the ionic species of the buffer and the analyte in the mobile phase with the highly charged surface. As the experimental sensitivity analysis suggests (Section 4.1.3), tracer amounts of the co-ions are considered in the calculations to keep the contribution to the ionic strength neglectable.

Via the modified nonlinear Poisson-Boltzmann equation, we calculate the length for the double layer for different co-ion species under different buffer conditions and compare them with the length that is derived from the retention times of the chromatographic negative adsorption experiments. Fig. 4 shows experimental and theoretical results of oxalate for different ionic strength and pH of the phosphate buffer. The scale of the ionic strength is logarithmic. Thereby, it demonstrates a proper investigation of the mechanism for up to two orders of magnitudes. The intensity of the chromatographic signal from minor relative peak areas (bright marker) to major relative peak areas (dark marker) is shown in the derived experimental length. The length is a negative value, since it derives from the negative derivative (dq_i/dc_i) for co-ions. Finally, the corresponding thickness of the double layer lies in the range of 3 to 11 nm. It is shown that the length decreases nonlinearly as the ionic strength increases. For low ionic strength, the change of the length of the double layer is greater than at high ionic strengths. The change of the pH at high ionic strength does not change the expansion of the double layer sensitively, as high concentrations of the counterion on the strong ion exchanger establish thinner double layers.

In the order of hundreds of millimolar, the apparent double layer thickness approximates the value of 2 nm, which is the thickness of the condensed layer of the counterions of finite size. While more complicated equations of state can be applied, the Bikerman model describes already well the complete experimental data set under consideration of the size of the counterion potassium. It is quite remarkable how the agreement of experimental and theoretical results shows how the theory self-consistently connects the microscopic adsorption mechanism and the macroscopic separation process; thereby, the ion size of a few Angstrom affects the chromatographic process, which operates in the length scale of decimeters.

At the two different conditions, pH 7 and pH 8, the self-consistent theory fits the experimental data well and is able to capture the nonlinear dependency of the length of the electric double layer and the co-ion repulsion on ionic strength (Fig. 4). However, at weak buffer conditions at pH 6, oxalate establishes an equilibrium of divalent and monovalent species as it is also indicated in the chromatograms. Therefore, two experimental lengths derive at the same ionic strength. At pH 8, the buffer conditions are not strong either but no monovalent oxalate species emerge due to oxalate's low pKa_2 value.

To interpret the result at pH 6, the theoretical result indicates two limits where the two solid lines show the limit of slow association of the charged species. Here, the divalent species is greater repelled than the

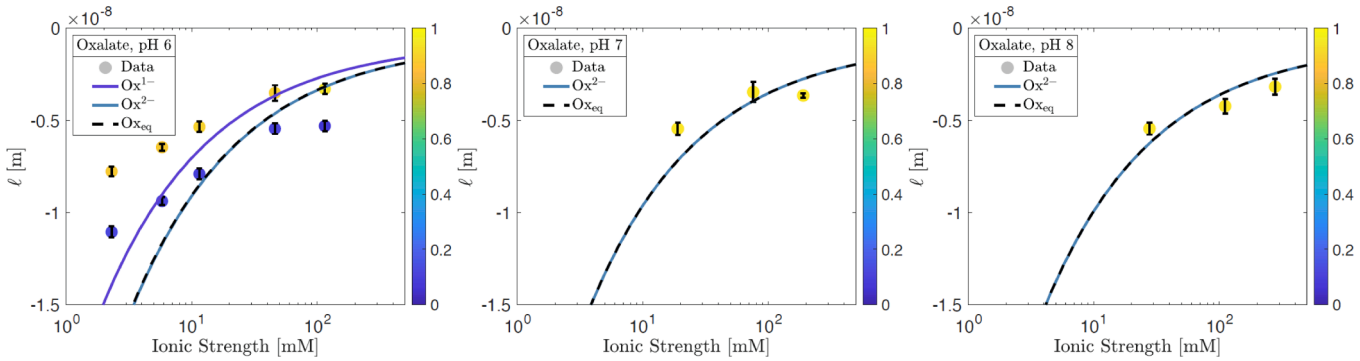

Fig. 4. Lengths ℓ of the valency species of the oxalate co-ion in respect of pH 6, 7 and 8 that indicate the thickness of the EDL according to negative adsorption in the chromatographic column. The values of the length are negative due to the exclusion of the co-ions from the double layer. Relative intensities of the chromatographic data go from major signal (bright marker) to minor signal (dark marker). Error bars indicate the propagated error as standard deviations from the retention time shifts. The theoretical curves show the cases of slow associations (solid lines, greater co-ion valency is the bottom line) and fast associations (dashed line). The phase ratio is $S = 1.6 \cdot 10^7$ m^{-1}. The crowding in the modified Poisson-Boltzmann equation is considered with the counterion size $a = 3.3$ Å.

monovalent although both indicate the same electrical double layer of accumulated counterions. The dashed line shows the other theoretical limit, where the equilibrium of the charged species according to the prevalent pH and the time shift is the population-weighted average of the time shifts. We point out that the solid line of the divalent species and the dashed line overlap at all pH values, which is in accordance to the pKa_2 value of oxalate. Thereby, the theory clearly identifies that the prevalent species at pH 7 and 8 is divalent while the second theoretical limit explains the occurrence of divalent and monovalent oxalate species.

The proposed interpretation of an apparent equilibrium (2-/1-) at weak buffer conditions is supported by the results of citrate, where the prevalence of the charged species even changes within investigated pH conditions around citrate's dissociation constant $pKa_3 = 6.40$ (Section 4.2.4). In these cases, the ineffectiveness of the buffer at low ionic strength leads to slight intrinsic pH gradients, which could be responsible for the peak splitting. Therefore, the different peaks incorporate different charge equilibria within. In the end, the expected result falls in between the two limits we explored with the theory. While the self-consistent theory overestimates the repulsion at very low ionic strengths below 10 mM, the resulting solution space that is spun by the two limits describes quite well the experimental data at pH 6 for two orders of magnitude of the ionic strength.

4.2.3. *Elucidation of transport phenomena: repulsion of citrate at pH 7 and 8*

For citrate, peak splitting occurs at any buffer condition (Fig. 5). The theoretical result shows that the prevalence changes from majorly divalent to trivalent species as the pH increases from pH 6 to pH 8, by then the limit of the equilibrium (dashed line) moves relatively to the limit of no equilibrium (solid lines) from the pure divalent to the pure trivalent species. At pH 8 better than at pH 7, the theory fits the major signal of the experimental data (bright markers) well and is able to capture the nonlinear dependency of the thickness of the electrical double layer and the co-ion repulsion on ionic strength. At high ionic strengths above 0.1 M at all pH values, the minor signal agrees more poorly with the theory as the two theoretical limits come relatively close together under these conditions. The deviation of theory and experiment may be accounted to an increased dependence of pKa_3 on ionic strength. Accordingly, the consideration of an activity coefficient to account for the influence of the ionic strength leads to a deviated dissociation constant pKa' of the carboxylic acid that is lower than pKa [48]. Thus, the kinetics change with increasing ionic strength at all pH conditions by favoring dissociation of the co-ion species over association. As the interplay of the kinetics altogether is very complex in IEC, the changing kinetics influence the accuracy of the model apparently at ionic strengths above 0.1 M. In fact, this highlights another contribution to the negative adsorption and would further increase the complexity at strong buffer conditions. However, our model qualitatively covers the emergence of the small signal by the limit of slow association.

Alike, only a qualitative distinction between the (3-/2-) equilibrium of citrate and the purely divalent species of oxalate can be made at pH 7 and pH 8. At pH 6, the picture is quite different with a third length at low ionic strength that derives from a third citrate peak in the chromatogram

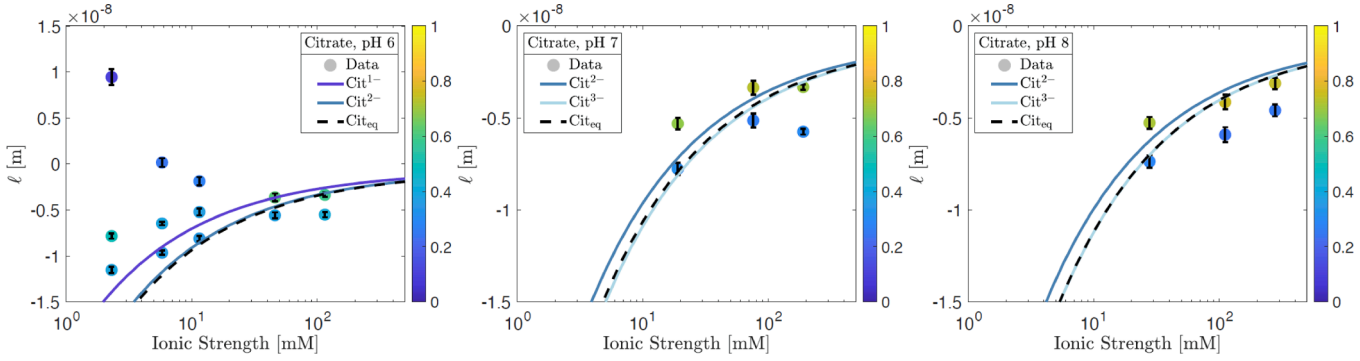

Fig. 5. Lengths ℓ of the valency species of the citrate co-ion in respect of pH 6, 7 and 8 that indicate the thickness of the EDL according to negative adsorption in the chromatographic column. Relative intensities of the chromatographic data go from major signal (bright marker) to minor signal (dark marker). Error bars indicate the propagated error as standard deviations from the retention time shifts. The theoretical curves show the cases of slow associations (solid lines, greater co-ion valency is the bottom line) and fast associations (dashed line). The phase ratio is $S = 1.6 \cdot 10^7$ m^{-1}. The crowding in the modified Poisson-Boltzmann equation is considered with the counterion size $a = 3.3$ Å.

(see Supporting Information) and, as we point out, the prevalence of other co-ion equilibria than in the case of pH 7 and 8. In Section 4.2.4, we thoroughly elaborate the possible reasons underlying this result.

4.2.4. Elucidation of transport phenomena: repulsion of citrate at pH 6

As exemplified in the chromatograms of oxalate (Fig. 2) and citrate (Fig. 3) at pH 6, the retention time shifts and the derived lengths for the two peaks are the same for any ionic strength with remarkable significance (more examples in Supporting Information). For this reason, it is possible to identify the co-ion equilibrium of the occurring species. Since oxalate cannot establish trivalent species and matches the citrate lengths, we presume that the citrate species have to be monovalent and divalent. Therefore, only the theoretical limit of monovalent and divalent species (solid lines) is relevant (Fig. 5). Here, the limit of the equilibrium (dashed line) is already close to the case of divalent citrate ions.

In this context, another interpretation indicates the occurrence of the third peaks, hence third length values, at low ionic strength. The experimental data points are pictured on a contrast scale from small peak area (dark marker) to great peak area (bright marker). Here, oxalate only establishes a small first peak (Fig. 2) and therefore, the data points are dark (Fig. 4). For citrate, at high ionic strength of any pH value, the first peak (more repulsion) is also always smaller than the second peak (less repulsion) (Fig. 5). However, at pH 6 and low ionic strength, the peak area is more balanced between the first and the second peak while also a small third peak appears. A way to interpret these features is that the equilibria at the other conditions are well established compared to the equilibrium at weak buffer conditions in terms of pH as well as ionic strength. Here, in addition to the already complex kinetics another effect occurs that leads to the third peak. The small length at 12 mM ionic strength indicates little repulsion, while at 6 mM, the length is zero, what means, that there is no repulsion. And at 2 mM, the length is even positive, which indicates positive adsorption onto the stationary phase. It means that some percentage of the citrate is not negatively charged or has a strong specific, non-electrostatic interaction that is not captured in our model. The experimental observation can be accounted to the formation of an additional equilibrium of monovalent and neutral species. This result strongly agrees with the working principle of ion exclusion chromatography to separate carboxylic acids.

Ion exclusion chromatography is most commonly used to separate carboxylic acids [49]. Strong cation-exchangers are used to separate carboxylic acids according to their pKa_1 value and to non-electrostatic interaction of the aliphatic rest of different size [50,51]. The mobile phase is normally water and consequently, the weak acids form an equilibrium of monovalent and neutral species. An addition of small concentrations of 5 mM of e.g., benzoic acid, to the mobile phase can be used to tune the equilibrium and more consistently support the formation of the monovalent species to obtain sharper peaks [50].

In general, the mobile phase in ion exclusion chromatography is not buffering and the equilibrium forms according to the pKa_1 value of the weak acid. This is comparable to the conditions with phosphate buffer at pH 6 and low ionic strengths. In accordance to the mechanism of the separation of carboxylic acids in ion exclusion chromatography, we deduce that the equilibrium of monovalent and neutral species forms in addition to the equilibrium of divalent and monovalent species. Consequently, pH gradients possibly occur in the column when the buffer is not functioning properly. Moreover, it is indicated that the equilibrium determined by pKa_1 influences the third length value more the lower the ionic strength (Fig. 5). The lower the ionic strength, the more the length increases, even leading to a change from negative to positive length values. In this way, adsorption of the neutral charge intensifies. In other words, the retention time increases the more neutral species adsorbs that underlies positive adsorption kinetics. Ultimately, the kinetic interplay gets even more complicated for citrate at weak buffer conditions.

The adsorption of neutral species may also apply to the tracer glucose and increase the reference elution time in the experimental dataset. Contrarily, the reference time decreases as glucose is sterically repelled from the condensed layer. Hereby, we are interpreting the experiments as if the volume of glucose is neglectable while the sensitivity to the packing constraints in the condensed layer is low (data not shown). The apparent double layer expansions would increase and decrease, respectively. Both effects may balance out, which ultimately leads to a good agreement of theory and experiment.

In the end, the underlying complex kinetics follow the interplay of co-ion repulsion of different charge species, two water association reactions with pKa_2 and pKa_1 and positive adsorption of the neutral species. In conclusion, the microscopic adsorption model explains the retention in the macroscopic separation process, and especially well at ionic strengths between 10 and 100 mM. In the investigated framework of this work, the electrostatic adsorption mechanism in the system is merely characterized by the determination of the solid surface charge and the consideration of the counterion size.

Moreover, an increase of pKa_1 values leads to more positive adsorption in ion exclusion chromatography of weak carboxylic acids [50]. This is important to complete the coherent interpretation of our results. Concretely, we compare the results of citrate and oxalate at weak buffer conditions. We derive that oxalate does not establish a neutral species (Fig. 3) and base it on the fact that its $pKa_1 = 1.46$ is much lower than the pKa_1 value of citrate with 3.13. Therefore, the buffer at pH 6 is still strong enough to repress neutral oxalate species but too weak to suppress neutral citrate species.

4.2.5. Application: comparison to SD model

Our work provides evidence supporting the conclusions made by Kopaciewicz *et al.* regarding protein adsorption, which ultimately contributed to the formulation of the SD model. First, the authors also investigated the interaction range of the solid surface for varying ionic strength of the buffer but only indirectly compared it to the EDL theory. In combination with further results, they deduced that a constant characteristic charge of the protein is established under eluting conditions of high ionic strength and, validated this phenomenon with protein adsorption experiments. Concretely, Kopaciewicz *et al.* experimentally examined the desorption of proteins on a strong IEC with sodium chloride concentrations in the order of a few 100 mM. Then, they formulated an empirical model that relates the capacity factor in chromatography to a constant characteristic charge – defined in the model – and the concentration of sodium chloride ions. Consequently, a methodology is derived that enables the experimental determination of the characteristic charge for linearly adsorbing proteins. However, the value of the characteristic charge is only valid for one type of stationary phase at eluting conditions and, only one type of buffer. As further understanding of the mechanism is missing, knowledge transfer is restricted from one system to another.

Our study elucidates the connection between the electrolyte conditions and the adsorption characteristics for a given surface charge. As our experimental and theoretical results show, eluting conditions for proteins would be in the upper range of the ionic strength that we investigated. Corresponding to the various co-ion equilibria in this regime, the thickness of the EDL does not change and approaches the thickness of the condensed layer as the ionic strength is increases (Fig. 4 and Fig. 5). As the size of the double layer under eluting conditions stays nearly the same, the interaction of the stationary surface with the protein assumingly stays the same. Therefore, it is reasonable that the empirically derived characteristic charge of the protein in the SD model, which phenomenologically lumps together the electrostatic effects, stays constant at eluting conditions. In other words, we can give an explanation what physical characteristics of the stationary phase, the electrolyte and the protein led to the success of the empirical SD model and are able to identify the regime where eluting conditions with a constant characteristic charge of the protein occur.

4.2.6. Application: significance of continuum-based model for desorption and adsorption in bioseparation systems

Potentially, the elucidation of the adsorption mechanism in IEC helps to design separation systems based on physical properties of the electrolyte and the stationary phase, like charge and pore size. Via the presented methodology, the behavior of the electrostatic interaction can be expressed by the derivative partition coefficient as a measure of the EDL thickness. Consequently, adsorption and desorption conditions in dependence on the ionic strength of the buffer can be determined for a system and compared to other systems by determination of the surface charge and consideration of the counterion size. For each system, the regime of greater sensitivity at low ionic strength and the regime of lower sensitivity at high ionic strength can be identified. Concretely, our results (Fig. 4 and Fig. 5) exemplarily show that the sensitivity of the EDL thickness is greater at ionic strengths roughly below 50 mM than above 50 mM. Ultimately, charged surfaces can be characterized and compared towards their electrostatic interaction behavior with various electrolyte conditions. In Section 4.2.5, we already have shown that our findings give an explanation for the successful applicability of the SD model under desorption conditions. On the other hand, greatest adsorption probabilities onto the stationary phase can theoretically be reached by maximal interaction volume of EDL thickness times surface area. In the following, we elaborate the findings in context of the adsorption of biological colloids.

In case of proteins, the concentration of the adsorption buffer in bioseparation systems is in the range of a few mM to a few cM. In this context, we estimate a trade-off between high buffer concentrations for a robust protein charge and low buffer concentrations for maximal electrostatic interaction. Here, the lower the ionic strength, the greater is the EDL and the higher the probability of interaction. Thereby, the design of the adsorption buffer in terms of electrostatic interaction can be quite sensitive in the order of millimolars and indicates potential for optimization. On the other hand, desorption conditions may already be reached at ionic strengths of 50 mM and above as the EDL thickness does not change much if the surface charge is high and a condensed layer of counterions is present. Here, a chance to resource reduction emerges by application of less elution salt.

We have shown that electrostatic adsorption in chromatography under biotechnological conditions can be described by a continuum model and therefore, we are able to put the EDL into context to pore sizes and protein sizes. Therefore, we estimate maximal Debye lengths in the pores from the optimized adsorption conditions of proteins. The underlying concentration regime of a few millimolar leads to Debye lengths of a few nanometers in case of monovalent counterions. Next, it is interesting to compare the length scale of electrostatic interaction to the length scale of hydrodynamic interaction and identify constraints in resin design and operating conditions. It is known that protein chromatography is diffusion-limited. Thereby, diffusion in the pores is hindered once the solute is too big. Macroscopic diffusivity of uncharged particles in cylindrical pores is reduced by somewhat 60 % compared to the bulk diffusivity when the ratio particle/pore radius is 1:5 [52]. For proteins of radii 2–10 nm, that means pore radii of 10–50 nm with such a reduced diffusivity. This exemplary result suggests that the pore sizes should not be decreased much further, as the diffusivity decreases greatly with increasing protein/pore size ratio. Thus, the hydrodynamic interaction determines the pore size in case of protein adsorption rather than the electrostatic interaction, as the corresponding length scale is one order of magnitude greater than the Debye length. In terms of material design, the trade-off for pore sizes is between great pores with unhindered hydrodynamic interaction and small pores with maximal surface area.

In conclusion, the concentration of adsorption buffers can be as low as possible as long as sufficient buffering of the protein is guaranteed. Under the constraints of hydrodynamic hindrance, the EDL spans across the pore surface what optimally affects protein adsorption. On the other hand, no overlapping of the EDL occurs that may change the accessibility of proteins to the pores, diffusion within the pores and the native state of the proteins.

The charge- and size-related interpretation in macroporous systems also holds qualitatively for other bioproducts that are purified via IEC, as there are plasmid DNA [53], virus-like particles [54], lipid or polymeric nanoparticles [55] and viral vectors [56].

5. Conclusion

In this work, we elaborate the physicochemical interplay of pH and ionic strength of the buffer with carboxylic acids in a strong cation-exchanger. From negative adsorption experiments, we derive retention times of the carboxylic acids at different ionic strengths and pH values of the mobile phase which leads to characterization of the interaction of ions with the resin. Subsequently, we identify how different charge species of oxalate and citrate are repelled from the highly charged surface. Thereby, we deploy a modified Poisson-Boltzmann theory to quantify and validate the observations made in the chromatography studies. While the EDL structure is determined by electrostatic adsorption and crowding of the buffer counterion of finite size, the length of the double layer is indicated by different co-ion charge species of the carboxylic acids. While more sophisticated models could be employed to incorporate the ion sizes, the mean-field formulation by Bikerman [34] already agrees well with the experimental data. We elaborated that the degree of repulsion is unspecific regarding the molecule type, but depends on the valency of the carboxylate co-ions. Our self-consistent theory provides an *a priori* explanation on the unfolding of electrostatic adsorption in the continuum of the chromatographic column. In detail, we summarize five aspects for the interplay of co-ions with the electrolyte and the stationary phase in the actual chromatographic process:

1. The greater the EDL expansion, which establishes at low counterion concentration, the greater is the repulsion of oxalate and citrate co-ions of the same valency.
2. The greater the co-ion valency, the more the co-ion is repelled, leading to a greater effective double-layer thickness for that co-ion.
3. The equilibrium of two co-ion valencies manifests itself as peak splitting. Behind it, the complex formation of co-ion charge species bases on the kinetics of co-ion repulsion from the surface and the kinetics of the water association reaction or intrinsic pH gradients.
4. The greater the difference of the pH value of the buffer from the pKa value of the buffer, the more the co-ion species are determined by the pKa values of oxalate and citrate.
5. For a weak buffer, with low ionic strength and the pH value far away from the pKa value of the buffer, conditions as in ion exclusion are set. Neutral species of citrate ($pKa_1 = 3.13$) form and adsorb to the stationary phase.

As others did for technical application like capacitive deionization and shock electrodialysis [24], we managed to pave the way to base process and material design in ion chromatography on surface exchange. Also, knowledge transfer from one system to another is enabled through physicochemical characterization of the separation system. The elucidation of the adsorption mechanism in ion chromatography may be beneficial to obtain higher resolutions in ion exclusion chromatography when the surface within the pores also contributes to the repulsion volume as well as optimized adsorption conditions and desorption conditions in ion exchange chromatography. Moreover, the experimental methodology via chromatography facilitates the characterization of charged materials in a high throughput setup under buffer conditions. Via the mechanistic model, the interplay of the electrolyte composition and ion exchange capacity are brought together. Finally, these investigations may not only be feasible for small ions, but also biomolecules and particles.

CRediT authorship contribution statement

G.M. Essert: Conceptualization, Investigation, Methodology, Software, Writing – original draft. **J.P. de Souza:** Methodology, Software, Writing – review & editing. **S.P. Schwaminger:** Supervision, Writing – review & editing. **M.Z. Bazant:** Funding acquisition, Supervision, Writing – review & editing. **S. Berensmeier:** Funding acquisition, Resources, Supervision, Writing – review & editing.

Declaration of competing interest

The authors declare the following financial interests/personal relationships which may be considered as potential competing interests: Gregor Markus Essert reports travel was provided by Massachusetts Institute of Technology International Science and Technology Initiatives. J. Pedro de Souza reports travel was provided by Massachusetts Institute of Technology International Science and Technology Initiatives. Martin Zdenek Bazant reports travel was provided by Massachusetts Institute of Technology International Science and Technology Initiatives. Sonja Berensmeier reports travel was provided by Massachusetts Institute of Technology International Science and Technology Initiatives. If there are other authors, they declare that they have no known competing financial interests or personal relationships that could have appeared to influence the work reported in this paper.

Data availability

Data will be made available on request.

Acknowledgments

The authors would like to acknowledge the MIT-Germany Lockheed Martin Seed Fund in addition to MIT International Science and Technology Initiatives (MISTI). We appreciate the support from Laura Capogrosso for undergoing chromatographic experimental work and data collection. We thank Stefan Rauwolf for assisting in chromatographic experiments and Prasika Arulrajah and Dennis Röcker for performing measurements of the specific surface area.

Appendix A. Supplementary data

Supplementary data to this article can be found online at https://doi.org/10.1016/j.seppur.2024.126860.

References

[1] N.R. Amundson, A note on the mathematics of adsorption in beds, J. Phys. Chem. 52 (1948) 1153–1157, https://doi.org/10.1021/j150463a007.
[2] L. Lapidus, N.R. Amundson, Mathematics of adsorption in beds. VI. The effect of longitudinal diffusion in ion exchange and chromatographic columns, J. Phys. Chem. 56 (1952) 984–988, https://doi.org/10.1021/j150500a014.
[3] N.R. Amundson, Mathematical methods in chemical engineering, Prentice-Hall, Englewood Cliffs, N.J., 1966.
[4] F.S. Bates, R. Neal, Amundson, a bold and brilliant leader of chemical engineering, Proc. Natl. Acad. Sci. U. S. A. 108 (2011) 7285, https://doi.org/10.1073/pnas.1104732108.
[5] E.V. Dydek, M.Z. Bazant, Nonlinear dynamics of ion concentration polarization in porous media: the leaky membrane model, AIChE J. 59 (2013) 3539–3555, https://doi.org/10.1002/aic.14200.
[6] V. Kumar, A.M. Lenhoff, Mechanistic modeling of preparative column chromatography for biotherapeutics, Annu. Rev. Chem. Biomol. Eng. 11 (2020) 235–255, https://doi.org/10.1146/annurev-chembioeng-102419-125430.
[7] W. Kopaciewicz, M.A. Rounds, J. Fausnaugh, F.E. Regnier, Retention model for high-performance ion-exchange chromatography, J. Chromatogr. A 266 (1983) 3–21, https://doi.org/10.1016/S0021-9673(01)90875-1.
[8] D. Roush, D. Asthagiri, D.K. Babi, S. Benner, C. Bilodeau, G. Carta, P. Ernst, M. Fedesco, S. Fitzgibbon, M. Flamm, J. Griesbach, T. Grosskopf, E.B. Hansen, T. Hahn, S. Hunt, F. Insaidoo, A. Lenhoff, J. Lin, H. Marke, B. Marques, E. Papadakis, F. Schlegel, A. Staby, M. Stenvang, L. Sun, P.M. Tessier, R. Todd, E. von Lieres, J. Welsh, R. Willson, G. Wang, T. Wucherpfennig, O. Zavalov, Toward in silico CMC: an industrial collaborative approach to model-based process development, Biotechnol. Bioeng. 117 (2020) 3986–4000, https://doi.org/10.1002/bit.27520.
[9] D.K. Babi, J. Griesbach, S. Hunt, F. Insaidoo, D. Roush, R. Todd, A. Staby, J. Welsh, F. Wittkopp, Opportunities and challenges for model utilization in the biopharmaceutical industry: current versus future state, Curr. Opin. Chem. Eng. 36 (2022) 100813, https://doi.org/10.1016/j.coche.2022.100813.
[10] P.M. Biesheuvel, M.Z. Bazant, Nonlinear dynamics of capacitive charging and desalination by porous electrodes, Phys. Rev. E Stat. Nonlinear Soft Matter Phys. 81 (2010) 31502, https://doi.org/10.1103/PhysRevE.81.031502.
[11] P.M. Biesheuvel, Y. Fu, M.Z. Bazant, Diffuse charge and Faradaic reactions in porous electrodes, Phys. Rev. E Stat. Nonlinear Soft Matter Phys. 83 (2011) 61507, https://doi.org/10.1103/PhysRevE.83.061507.
[12] P.M. Biesheuvel, Y. Fu, M.Z. Bazant, Electrochemistry and capacitive charging of porous electrodes in asymmetric multicomponent electrolytes, Russ. J. Electrochem. 48 (2012) 580–592, https://doi.org/10.1134/S1023193512060031.
[13] P.M. Biesheuvel, H.V.M. Hamelers, M.E. Suss, Theory of water desalination by porous electrodes with immobile chemical charge, Colloids Interface, Sci. Commun. 9 (2015) 1–5, https://doi.org/10.1016/j.colcom.2015.12.001.
[14] P.M. Biesheuvel, S. Porada, M. Levi, M.Z. Bazant, Attractive forces in microporous carbon electrodes for capacitive deionization, J. Solid State Electrochem. 18 (2014) 1365–1376, https://doi.org/10.1007/s10008-014-2383-5.
[15] F. He, P.M. Biesheuvel, M.Z. Bazant, T.A. Hatton, Theory of water treatment by capacitive deionization with redox active porous electrodes, Water Res. 132 (2018) 282–291, https://doi.org/10.1016/j.watres.2017.12.073.
[16] X. Su, T.A. Hatton, Redox-electrodes for selective electrochemical separations, Adv. Colloid Interface Sci. 244 (2017) 6–20, https://doi.org/10.1016/j.cis.2016.09.001.
[17] A. Hemmatifar, M. Stadermann, J.G. Santiago, Two-dimensional porous electrode model for capacitive deionization, J. Phys. Chem. C 119 (2015) 24681–24694, https://doi.org/10.1021/acs.jpcc.5b05847.
[18] A.N. Shocron, I. Atlas, M.E. Suss, Predicting ion selectivity in water purification by capacitive deionization: electric double layer models, Curr. Opin. Colloid Interface Sci. 60 (2022) 101602, https://doi.org/10.1016/j.cocis.2022.101602.
[19] R. Zhao, M. van Soestbergen, H.H.M. Rijnaarts, A. van der Wal, M.Z. Bazant, P. M. Biesheuvel, Time-dependent ion selectivity in capacitive charging of porous electrodes, J. Colloid Interface Sci. 384 (2012) 38–44, https://doi.org/10.1016/j.jcis.2012.06.022.
[20] R. Wagner, S. Winger, M. Franzreb, Predicting the potential of capacitive deionization for the separation of pH-dependent organic molecules, Eng. Life Sci. 21 (2021) 589–606, https://doi.org/10.1002/elsc.202100037.
[21] E.V. Dydek, B. Zaltzman, I. Rubinstein, D.S. Deng, A. Mani, M.Z. Bazant, Overlimiting current in a microchannel, Phys. Rev. Lett. 107 (2011) 118301, https://doi.org/10.1103/PhysRevLett.107.118301.
[22] D. Deng, E.V. Dydek, J.-H. Han, S. Schlumpberger, A. Mani, B. Zaltzman, M. Z. Bazant, Overlimiting current and shock electrodialysis in porous media, Langmuir 29 (2013) 16167–16177, https://doi.org/10.1021/la4040547.
[23] K.M. Conforti, M.Z. Bazant, Continuous ion-selective separations by shock electrodialysis, AIChE J. 66 (2020) 1490, https://doi.org/10.1002/aic.16751.
[24] M.A. Alkhadra, X. Su, M.E. Suss, H. Tian, E.N. Guyes, A.N. Shocron, K.M. Conforti, J.P. de Souza, N. Kim, M. Tedesco, K. Khoiruddin, I.G. Wenten, J.G. Santiago, T. A. Hatton, M.Z. Bazant, Electrochemical methods for water purification, ion separations, and energy conversion, Chem. Rev. 122 (2022) 13547–13635, https://doi.org/10.1021/acs.chemrev.1c00396.
[25] H. Tian, M.A. Alkhadra, K.M. Conforti, M.Z. Bazant, Continuous and selective removal of lead from drinking water by shock electrodialysis, ACS EST Water 1 (2021) 2269–2274, https://doi.org/10.1021/acsestwater.1c00234.
[26] H. Tian, M.A. Alkhadra, M.Z. Bazant, Theory of shock electrodialysis II: mechanisms of selective ion removal, J. Colloid Interface Sci. 589 (2021) 616–621, https://doi.org/10.1016/j.jcis.2020.11.127.
[27] H. Tian, M.A. Alkhadra, M.Z. Bazant, Theory of shock electrodialysis I: water dissociation and electrosmotic vortices, J. Colloid Interface Sci. 589 (2021) 605–615, https://doi.org/10.1016/j.jcis.2020.12.125.
[28] M.A. Alkhadra, M.Z. Bazant, Continuous and selective separation of heavy metals using shock electrodialysis, Ind. Eng. Chem. Res. 61 (2022) 16240–16246, https://doi.org/10.1021/acs.iecr.2c02627.
[29] H.J. Van den Hul, J. Lyklema, Determination of specific surface areas of dispersed materials by negative adsorption, J. Colloid Interface Sci. 23 (1967) 500–508, https://doi.org/10.1016/0021-9797(67)90196-8.
[30] J. Lyklema, Fundamentals of Interface and Colloid Science. Volume I: Fundamentals, Academic Press, London, 1991.
[31] G. Guiochon, S.G. Shirazi, A.M. Katti, Fundamentals of Preparative and Nonlinear Chromatography, Academic Press, London, 1994.
[32] P. DePhillips, A.M. Lenhoff, Pore size distributions of cation-exchange adsorbents determined by inverse size-exclusion chromatography, J. Chromatogr. A 883 (2000) 39–54, https://doi.org/10.1016/S0021-9673(00)00420-9.
[33] J. Lyklema, Fundamentals of interface and colloid science, Volume II: Solid Liquid Interfaces (1995).
[34] J.J. Bikerman XXXIX, Structure and capacity of electrical double layer, Philos. Mag. 33 (1942) 384–397, https://doi.org/10.1080/14786444208520813.
[35] T.B. Grimley, N.F. Mott, I. General and theoretical. The contact between a solid and a liquid electrolyte, Discuss. Faraday Soc. 1 (1947) 3–11, https://doi.org/10.1039/df9470100003.
[36] M.Z. Bazant, M.S. Kilic, B.D. Storey, A. Ajdari, Towards an understanding of induced-charge electrokinetics at large applied voltages in concentrated solutions, Adv. Colloid Interface Sci. 152 (2009) 48–88, https://doi.org/10.1016/j.cis.2009.10.001.

[37] Y. Han, S. Huang, T. Yan, A mean-field theory on the differential capacitance of asymmetric ionic liquid electrolytes, J. Condens. Matter Phys. 26 (2014) 284103, https://doi.org/10.1088/0953-8984/26/28/284103.
[38] M. McEldrew, Z.A.H. Goodwin, A.A. Kornyshev, M.Z. Bazant, Theory of the double layer in water-in-salt electrolytes, J. Phys. Chem. Lett. 9 (2018) 5840–5846, https://doi.org/10.1021/acs.jpclett.8b02543.
[39] Z.A.H. Goodwin, J.P. de Souza, M.Z. Bazant, A.A. Kornyshev, Mean-field theory of the electrical double layer in ionic liquids, in: S. Zhang (Ed.), Encyclopedia of Ionic Liquids, Springer, Singapore, 2021, pp. 1–13.
[40] J.J. López-García, J. Horno, C. Grosse, Poisson-Boltzmann description of the electrical double layer including ion size effects, Langmuir 27 (2011) 13970–13974, https://doi.org/10.1021/la2025445.
[41] M. Schulte, M. Jöhnck, R. Skudas, K.K. Unger, von Hohenesche, Cedric du Fresne, W. Wewers, Dingenen Jules, Kinkel Joachim, Stationary Phases and Chromatographic Systems, in: H. Schmidt-Traub, M. Schulte, A. Seidel-Morgenstern (Eds.), Preparative Chromatography, second ed., Wiley-VCH, Weinheim, 2012, pp. 47–198.
[42] W.M. Deen, Analysis of Transport Phenomena, second ed., Oxford University Press, 2011.
[43] M.J. O'Neil (Ed.), The Merck Index – An Encyclopedia of Chemicals, Drugs, and Biologicals, Whitehouse Station, Merck and Co., Inc., NJ, 2006.
[44] David R. Lide (Ed.), CRC Handbook of Chemistry and Physics, Internet Version 2005, CRC Press, Boca Raton, FL, 2005. <http://www.hbcpnetbase.com>.
[45] G.D. Clayton, F.E. Clayton (Eds.), Volume 2A, 2B, 2C: Toxicology, John Wiley Sons, New York, 1981.
[46] B. Guélat, G. Ströhlein, M. Lattuada, M. Morbidelli, Electrostatic model for protein adsorption in ion-exchange chromatography and application to monoclonal antibodies, lysozyme and chymotrypsinogen A, J. Chromatogr. A 1217 (2010) 5610–5621, https://doi.org/10.1016/j.chroma.2010.06.064.
[47] J.N. Israelachvili, Intermolecular and Surface Forces, third ed., Academic Press, 2011.
[48] A.B. Hastings, J. Sendroy, The effect of variation in ionic strength on the apparent first and second dissociation constants of carbonic acid, J. Biol. Chem. 65 (1925) 445–455, https://doi.org/10.1016/S0021-9258(18)84852-9.
[49] P.R. Haddad, P.E. Jackson, Ion Chromatography, Elsevier, Amsterdam, 1990.
[50] K. Tanaka, J.S. Fritz, Separation of aliphatic carboxylic acids by ion-exclusion chromatography using a weak-acid eluent, J. Chromatogr. A 361 (1986) 151–160, https://doi.org/10.1016/S0021-9673(01)86902-8.
[51] K. Tanaka, T. Ishizuka, H. Sunahara, Elution behaviour of acids in ion-exclusion chromatography using a cation-exchange resin, J. Chromatogr. A 174 (1979) 153–157, https://doi.org/10.1016/s0021-9673(00)87045-4.
[52] W.M. Deen, Hindered transport of large molecules in liquid-filled pores, AIChE J. 33 (1987) 1409–1425, https://doi.org/10.1002/aic.690330902.
[53] M.M. Diogo, J.A. Queiroz, D.M.F. Prazeres, Chromatography of plasmid DNA, J. Chromatogr. A 1069 (2005) 3–22, https://doi.org/10.1016/j.chroma.2004.09.050.
[54] A. Zeltins, Construction and characterization of virus-like particles: a review, Mol. Biotechnol. 53 (2013) 92–107, https://doi.org/10.1007/s12033-012-9598-4.
[55] H. Yin, R.L. Kanasty, A.A. Eltoukhy, A.J. Vegas, J.R. Dorkin, D.G. Anderson, Non-viral vectors for gene-based therapy, Nat. Rev. Genet. 15 (2014) 541–555, https://doi.org/10.1038/nrg3763.
[56] C.E. Dunbar, K.A. High, J.K. Joung, D.B. Kohn, K. Ozawa, M. Sadelain, Gene therapy comes of age, Science 359 (2018), https://doi.org/10.1126/science.aan4672.